Optical line shapes of dynamically disordered ring aggregates

Lisette D. Bakalis, Mircea Coca, and Jasper Knoester

Citation: The Journal of Chemical Physics **110**, 2208 (1999); doi: 10.1063/1.477833
View online: http://dx.doi.org/10.1063/1.477833
View Table of Contents: http://scitation.aip.org/content/aip/journal/jcp/110/4?ver=pdfcov
Published by the AIP Publishing

Optical line shapes of dynamically disordered ring aggregates

Lisette D. Bakalis, Mircea Coca, and Jasper Knoester[a)]
Institute for Theoretical Physics and Materials Science Center, Nijenborgh 4, 9747 AG Groningen, The Netherlands

(Received 24 July 1998; accepted 23 October 1998)

We study the absorption line shape caused by Frenkel excitons in one-dimensional ring-shaped molecular aggregates, such as circular light-harvesting systems, subjected to dynamic disorder with a finite correlation time. We focus on dichotomic noise and show that for arbitrary orientations of the molecular transition dipoles relative to the ring, the absorption spectrum may be calculated exactly by solving two very similar sets of 2^N coupled linear equations of motion, where N is the number of molecules in the ring. These sets are a factor of N smaller than in methods developed previously, which allows us to evaluate the exact line shapes for N up to 12 and study size dependence of the spectra. Previous exact calculations were limited to hexamers ($N=6$). Moreover, in contrast to earlier work, we take into account long-range dipolar transfer interactions between all molecules in the ring. We find that the dipole orientation and the long-range interactions strongly affect the dependence of the spectrum on the ring size. This holds true particularly for the exchange narrowing of the linewidths in the fast-fluctuation regime. © *1999 American Institute of Physics.* [S0021-9606(99)70604-5]

I. INTRODUCTION

Since the recent discovery that several bacterial light-harvesting systems have a highly symmetric circular structure,[1] the interest in one-dimensional molecular ring aggregates has increased strongly. These light-harvesting systems contain rings with several tens (16-32) of chlorophyll molecules over which the electronic energy may be transported, before jumping to another ring or to a reaction center. Whether this transport is coherent (excitonlike) or incoherent (hoppinglike) is still a matter of much debate.[2–5] The amount of coherence and the exciton delocalization length over the ring depends crucially on the effect of the complex environment: random solvation shifts and scattering on vibrations affect the exciton dynamics. These processes are also reflected in the absorption spectrum of the system.

A simple level of modeling such effects, without addressing the environment in any detail, is to dress the exciton model with dynamic disorder. In this intuitively appealing model, each molecule is given a time-dependent frequency offset, determined by some stochastic process. This approach was originally introduced in the context of spin resonance experiments[6,7] and later applied to the optical response of (coupled) chromophores.[8–13] Although, strictly speaking, this model can only be justified for temperatures that are high compared to the frequency of the modes in the environment,[14,15] it has been used very successfully to describe ultrafast spectroscopies, involving fast bath modes, for single molecules in solution.[16] Two frequency scales govern the stochastic process: the amplitude (Δ) of the fluctuations and the fluctuation rate (λ). The third frequency scale that enters the problem is the intermolecular excitation transfer interaction (J_0). Owing to the occurrence of three different frequency scales, the calculation of any dynamic quantity of the system is very complicated. Except for limiting situations such as the static limit or the white noise limit ($\lambda \gg \Delta, J_0$),[8,17] one has to resort to approximate solutions. Examples of such approaches are the dynamic coherent potential approximation,[9] cumulant expansions,[10,11] decoupling schemes like the random phase approximation,[12] and simulation techniques to evaluate path integral expressions.[13]

An interesting type of stochastic process that allows for, at least numerically, exact solutions of the absorption spectrum, is dichotomic Markov noise. In this process, the random frequency offset of a molecule can take two values ($\pm\Delta$) and randomly jumps from one value to the other with an average rate λ. Reineker, Barvík, and co-workers[18,19] showed that for this process the absorption spectrum can be calculated by solving a closed hierarchy of $N2^N$ linear equations of motion, where N is the number of molecules in the aggregate. During recent years, these authors have applied this method to study the absorption spectra for $N=3$, 4, and 6 for a range of parameter values Δ/J_0 and λ/J_0. Recently,[20] we briefly reported on how for ring aggregates with dipoles oriented perpendicular to the plane of the ring, an alternative closed set of only 2^N equations of motion may be derived to calculate the absorption spectrum. This smaller set allowed us to calculate spectra for ring sizes up to $N=9$ and made it possible to study the phenomenon of exchange narrowing of fast fluctuations. The case $N=9$ may already be of interest to light-harvesting systems, as the antenna system LH2 of purple bacteria contains rings of eight or nine chlorophyll dimers.[1] However, in these systems, the molecular transition dipoles are known to basically lie in the plane of the ring.

In this paper, we therefore consider the general situation, where the molecular dipoles have arbitrary orientations relative to the ring. Moreover, we include all intermolecular transfer interactions on the rings. Previous calculations have

a)Electronic mail: knoester@chem.rug.nl

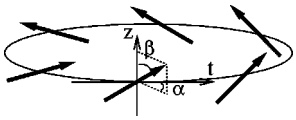

FIG. 1. Schematic representation of the ring aggregate. The thick arrows indicate the transition dipole moments of the individual molecules. For every molecule, the angle between its transition dipole and the normal to the plane of the ring (the z axis) equals β, while the angle between the projection of the dipole on the plane of the ring and the tangent t to the ring is denoted α.

been restricted to nearest-neighbor interactions, an approximation which for dipolar ($1/r^3$) interactions may be expected to be rather poor. We show that for this general situation, it is sufficient to solve two (very similar) closed sets of 2^N linear equations of motion in order to calculate the absorption spectrum. We apply our method to calculate spectra for rings consisting of up to $N=12$ molecules and focus in particular on the N dependence of the spectra. We show that exchange narrowing occurs independent of the orientation of the molecular dipoles, although the precise value of the narrowing factor and its large-aggregate saturation value *are* influenced by these orientations as well as by the long-range nature of the interactions.

The outline of this paper is as follows. In Sec. II, we define the model and express the absorption spectrum in terms of the stochastic average of one-exciton Green functions. In particular, the way the dipole orientations enter the intermolecular interactions and the expression for the spectrum will be clarified. In Sec. III, the two closed hierarchies of equations of motion that suffice to evaluate the absorption spectrum in the case of dichotomic noise will be derived. These equations are used in Sec. IV to evaluate the exact absorption spectra for various system sizes, dipole orientations, and values for Δ/J_0 and λ/J_0. A discussion of these results is given. In Sec. V we focus on the effect of exchange narrowing and the random phase approximation. Finally, in Sec. VI we summarize and briefly address the more general model, where the disorder also contains a purely static component in addition to a dynamic one.

II. MODEL AND ABSORPTION SPECTRUM

We consider a cyclic aggregate consisting of N equidistant two-level molecules arranged on a ring of radius R. The molecules have transition dipoles with magnitude μ that is equal for all molecules. The dipoles all have equal orientation relative to the ring: the angle between the dipoles and the normal to the plane of the ring is denoted β, while the angle between the projection of the dipole on the plane of the ring and the tangent to the ring is denoted α (Fig. 1). We indicate the plane of the ring as the xy plane and the direction perpendicular to the ring as the z direction. Thus, $\mu_z=\mu\cos\beta$ and $\mu_{xy}=\mu\sin\beta$. If we model the effect of the environment on the molecules by a stochastic modulation of the transition frequencies, the Frenkel exciton Hamiltonian for the aggregate reads ($\hbar=1$),

$$\hat{H}(t)=\sum_n\,[\omega_0+\Delta_n(t)]\hat{b}_n^\dagger\hat{b}_n+\sum_{n,m}J(m)\hat{b}_n^\dagger\hat{b}_{n+m}. \qquad (1)$$

Here, $\hat{b}_n^\dagger$ and $\hat{b}_n$ denote the Pauli creation and annihilation operator,[21,22] respectively, for an excitation on molecule n ($=0,1,\ldots,N-1$), ω_0 is the average molecular transition frequency, and $\Delta_n(t)$ is the modulation of the frequency of molecule n at time t. In the second term of the Hamiltonian, $J(m)$ is the intermolecular excitation transfer interaction between two molecules which are m lattice constants apart on the ring. Thus, $m=\pm1,\pm2,\ldots,$ until all molecules ($\neq n$) on the ring are accounted for, where periodic boundary conditions are implicit: $\hat{b}_{n+N}^\dagger=\hat{b}_n^\dagger$.

The transfer interactions result from the intermolecular dipole–dipole interactions and are given by

$$J(m)=J_0\left(\frac{\sin(\pi/N)}{\sin(\pi|m|/N)}\right)^3\{\cos^2\beta-\tfrac{1}{2}\sin^2\beta[\cos(2\pi m/N)+3\cos(2\alpha)]\}, \qquad (2)$$

where

$$J_0=\frac{\mu^2}{[2R\sin(\pi/N)]^3}=\frac{\mu^2}{a^3} \qquad (3)$$

is the interaction between two nearest-neighbor molecules if their dipoles μ would be oriented in the z direction (a is the nearest-neighbor distance on the ring). We note that J_0 is always positive. Whether the actual nearest-neighbor interaction on the ring is positive (H aggregate) or negative (J aggregate) depends on the orientation factor (i.e., the last factor) in Eq. (2). In the literature, $J(m)$ is mostly approximated by a nearest-neighbor interaction, i.e., only terms with $m=\pm1$ are kept; we will not make this approximation here.

We now turn to the description of the stochastic frequency modulation. We will assume that the $\Delta_n(t)$ are independent dichotomic Markov processes[19,23,24] of amplitude Δ and correlation time λ^{-1}. Thus at time t, each $\Delta_n(t)$ either has the value $+\Delta$ or $-\Delta$, while its correlation function decays according to:

$$\langle\Delta_m(t)\Delta_n(\tau)\rangle=\delta_{mn}\Delta^2e^{-\lambda|t-\tau|}. \qquad (4)$$

For large λ, the fluctuation varies rapidly between $+\Delta$ and $-\Delta$, whereas for $\lambda=0$ the model describes static dichotomic disorder. The case of finite λ is referred to as colored dichotomic noise.

More information about the dichotomic process and its correlation functions may be found in Ref. 23. Here we restrict ourselves to the property that is most important to evaluate the optical line shape of the aggregate: the differentiation rule. Clearly, any dynamic variable of the aggregate is a functional of the N frequency fluctuations $\{\Delta_i\}$. Let $\Phi_t[\{\Delta_i\}]$ be such a variable, where the functional dependence is denoted in the square brackets and the explicit time dependence through the subscript t. Then we have

$$\frac{d}{dt}\langle\Delta_1(t)\Delta_2(t)\cdots\Delta_k(t)\Phi_t[\{\Delta_i\}]\rangle=\left\langle\Delta_1(t)\Delta_2(t)\cdots\Delta_k(t)\frac{d}{dt}\Phi_t[\{\Delta_i\}]\right\rangle-k\lambda\langle\Delta_1(t)\Delta_2(t)\cdots\Delta_k(t)\Phi_t[\{\Delta_i\}]\rangle. \qquad (5)$$

This rule can be proven using functional Taylor expansion, as is done in Ref. 25 for the case of one dichotomic process. The generalization to N equivalent but independent processes is easily given. The second right hand side term in Eq. (5) results from the fact that multitime correlations of dichotomic fluctuations factorize into products of two-time correlation functions;[23] the latter decay exponentially with rate λ according to Eq. (4). We remark in passing that Eq. (5) also holds for Gauss–Markov fluctuations.

Next, we turn to the general expression for the linear absorption spectrum $I(\omega)$ of an ensemble of aggregates. According to standard linear response theory, this spectrum is determined by the two-time correlation function of its total transition dipole operator $\hat{\boldsymbol{\mu}}_n=\Sigma_n\boldsymbol{\mu}_n(\hat{b}_n^\dagger+\hat{b}_n)$, where $\boldsymbol{\mu}_n$ denotes the transition dipole of molecule n. Here, we use the fact that the aggregates are much smaller than an optical wavelength. Applying the rotating wave approximation, one arrives at the general expression

$$I(\omega)=\mathrm{Re}\int_0^\infty dt e^{i\omega t}\sum_{n,m=0}^{N-1}\langle(\mathbf{e}\cdot\boldsymbol{\mu}_n)(\mathbf{e}\cdot\boldsymbol{\mu}_m)\rangle_{\mathrm{or}}\langle U_{nm}(t)\rangle. \tag{6}$$

Here, $\mathbf{e}$ is the electric polarization vector of the absorbed light, $\langle\cdots\rangle_{\mathrm{or}}$ denotes the average over the orientations of the normal to the aggregate ring (the z axis) relative to this polarization vector, and $\langle\cdots\rangle$ denotes the average over the stochastic processes. Furthermore, $U_{mn}(t)$ are the one-exciton Green functions defined by

$$U_{nm}(t)\equiv\langle 0|\hat{b}_n\hat{U}(t)\hat{b}_m^\dagger|0\rangle, \tag{7}$$

where $\hat{U}(t)$ is the evolution operator obeying

$$d\hat{U}/dt=-i\hat{H}(t)\hat{U} \tag{8}$$

and $|0\rangle$ denotes the aggregate's ground state, in which all molecules are in the ground state. Using the fact that $\langle U_{nm}(t)\rangle=\langle U_{0,m-n}(t)\rangle$ (translational symmetry of disorder averages), Eq. (6) is easily reduced to

$$I(\omega)=\frac{N}{3}\mathrm{Re}\int_0^\infty dt e^{i\omega t}\sum_{n=0}^{N-1}[\mu_z^2+\mu_{xy}^2\cos(2\pi n/N)]\times\langle U_{0n}(t)\rangle, \tag{9}$$

where we assumed an isotropic orientational distribution of the rings, as is appropriate for solutions. The spectrum obeys the sum rule $\int_0^\infty I(\omega)d\omega=N\pi/3$.

It should be noted that Eq. (9) is not restricted to the dichotomic Markov process, but in fact holds for any stochastic frequency modulation. In Sec. III, we will show how in the special case of dichotomic Markov noise the absorption spectrum can be calculated starting from Eq. (9) and using the general rule, Eq. (5), to generate a closed hierarchy of equations of motions.

III. ABSORPTION SPECTRUM FOR DICHOTOMIC NOISE

For the special case of the dichotomic Markov process described in Sec. II, the variables $\Sigma_n\langle U_{0n}(t)\rangle$ and $\Sigma_n[\cos(2\pi n/N)\langle U_{0n}(t)\rangle]$ occurring in Eq. (9) can be calculated from closed hierarchies of equations of motion. This property was first utilized in Ref. 18 to calculate the absorption spectrum for dimers; applications to other oligomers (up to hexamers) have also been reported.[19] In this method, to calculate $\Sigma_n\langle U_{0n}(t)\rangle$, one derives its equation of motion, using Eq. (5). The Hamiltonian time evolution of $U_{0n}(t)$ [Eq. (8)] leads to new variables of the type $\Sigma_n\langle\Delta_m(t)U_{0n}(t)\rangle$, which in turn couples to $\Sigma_n\langle\Delta_{m_1}(t)\Delta_{m_2}(t)U_{0n}(t)\rangle$, etc. For dichotomic noise, this hierarchy of linear equations of motion eventually closes, because $\Delta_n(t)^2=\Delta^2$ for any n and any t.

Here, we use the same basic strategy to calculate the absorption spectrum. Our hierarchies have a simpler form, however, and also look much more similar for the z and the xy parts of the spectrum, because we explicitly use the cyclic nature of the system and the translational invariance of average quantities. This also allows us to reduce the size of the hierarchy from $N2^N$ equations to 2^N equations. Finally, our equations of motion also account for the long-range nature of the transfer interactions $J(m)$.

In Ref. 20 we already presented the set of 2^N variables that obeys a closed hierarchy of linear equations of motion for the case where the dipoles are oriented perpendicular to the plane of the ring. The set necessary to calculate the μ_z^2 part of the spectrum (i.e., $\Sigma_n\langle U_{0n}(t)\rangle$) is identical to that set. The fact that now we allow for arbitrary dipole orientations and long-range interactions only affects the equations of motion coupling these variables. The set contains the following variables:

$$X^{(0)}(t)\equiv\sum_{n=0}^{N-1}\langle U_{0n}(t)\rangle, \tag{10}$$

$$X^{(k)}(n_1,n_2,\ldots,n_k;t)\equiv\frac{1}{\Delta^k}\sum_{n=0}^{N-1}\langle U_{0n}(t)\Delta_{n_1}(t)\Delta_{n_2}(t)\cdots\Delta_{n_k}(t)\rangle, \tag{11}$$

where $1\leqslant k\leqslant N$ and $0\leqslant n_1<n_2<\cdots<n_k\leqslant N-1$.

Using Eq. (5) with $\Phi_t=\Sigma_nU_{0n}(t)$ and the Hamiltonian evolution, Eq. (8), one obtains the general equation of motion connecting the variables in this set:

$$\begin{aligned}\frac{d}{dt}X^{(k)}(n_1,n_2,\ldots,n_k;t)&=-(i\omega_0+k\lambda)X^{(k)}(n_1,n_2,\ldots,n_k;t)\\&\quad-i\sum_{m=\pm1,\pm2,\ldots}J(m)X^{(k)}(n_1-m,n_2-m,\ldots,n_k-m;t)\\&\quad-i\Delta(1-\delta_{n_1,0})X^{(k+1)}(0,n_1,n_2,\ldots,n_k;t)\\&\quad-i\Delta\,\delta_{n_1,0}X^{(k-1)}(n_2,\ldots,n_k;t).\end{aligned} \tag{12}$$

Here we used the translational invariance of averages:

$$\langle U_{mn}(t)\Delta_{n_1}(t)\Delta_{n_2}(t)\cdots\Delta_{n_k}(t)\rangle=\langle U_{0,n-m}(t)\Delta_{n_1-m}(t)\Delta_{n_2-m}(t)\cdots\Delta_{n_k-m}(t)\rangle. \tag{13}$$

The set of variables $X^{(k)}(t)$ defined above form a vector $\mathbf{X}(t)$ of dimension 2^N. As the first element of this vector, we use $X^{(0)}(t)$. The equation of motion for $\mathbf{X}(t)$ now reads

$$\frac{d}{dt}\mathbf{X}(t) = -i\mathbf{R}\mathbf{X}(t), \tag{14}$$

where the matrix $\mathbf{R}$ follows from Eq. (12), e.g., $R_{1,1} = \omega_0 + \Sigma_m J(m)$. It can easily be verified that this coefficient matrix is symmetric. The initial condition to Eq. (14) is: $X^{(0)}(t=0) = 1$, while all other components of $\mathbf{X}$ vanish at $t = 0$.

The hierarchy needed to calculate $\Sigma_n[\cos(2\pi n/N) \times \langle U_{0n}(t)\rangle]$ (the μ_{xy}^2 part of the spectrum) looks very similar to the one above. In this case, the 2^N independent variables are:

$$Y^{(0)}(t) \equiv \sum_n e^{-2\pi i n/N}\langle U_{0n}(t)\rangle, \tag{15}$$

$$Y^{(k)}(n_1, n_2, \ldots, n_k; t) \equiv \frac{1}{\Delta^k}\sum_n e^{-2\pi i n/N}\langle U_{0n}(t)\Delta_{n_1}(t)\Delta_{n_2}(t)\cdots\Delta_{n_k}(t)\rangle, \tag{16}$$

where $1 \leqslant k \leqslant N$ and $0 \leqslant n_1 < n_2 < \cdots < n_k \leqslant N-1$.

Here, it should be noted that due to the inversion symmetry of the average Green function, $\langle U_{0,-n}(t)\rangle = \langle U_{0,n}(t)\rangle$, the first variable in this set also equals $Y^{(0)}(t) = \Sigma_n[\cos(2\pi n/N)\langle U_{0n}(t)\rangle]$, which is the variable we need to calculate the spectrum. The equation of motion for $Y^{(k)}(t)$ has the same form as Eq. (12) (with each X replaced by the corresponding Y variable) except that the interaction $J(m)$ in the second right hand side term is replaced by $J(m)\exp(-2\pi i m/N)$.

Again, we form a vector $\mathbf{Y}(t)$ of dimension 2^N from the variables $Y^{(k)}(t)$ with first element $Y^{(0)}(t)$. The equation of motion for $\mathbf{Y}(t)$ reads

$$\frac{d}{dt}\mathbf{Y}(t) = -i\mathbf{S}\mathbf{Y}(t), \tag{17}$$

where the matrix $\mathbf{S}$ is identical to $\mathbf{R}$, except for the substitution of $J(m)$ by $J(m)\exp(-2\pi i m/N)$. The initial condition to Eq. (17) is: $Y^{(0)}(t=0) = 1$, while all other components of $\mathbf{Y}$ vanish at $t = 0$.

The total absorption spectrum [Eq. (9)] may now be written as

$$I(\omega) = \frac{N}{3}\mathrm{Re}[\mu_z^2\tilde{X}^{(0)}(\omega) + \mu_{xy}^2\tilde{Y}^{(0)}(\omega)], \tag{18}$$

where the tilde denotes the one-sided Fourier transform: $\tilde{f}(\omega) \equiv \int_0^\infty dt e^{i\omega t} f(t)$. Using Eqs. (14), (17), and (18) and the initial conditions, the final expression for the spectrum is

$$I(\omega) = -\frac{N}{3}\mathrm{Im}[\mu_z^2\{\omega\mathbf{1}-\mathbf{R}\}_{1,1}^{-1} + \mu_{xy}^2\{\omega\mathbf{1}-\mathbf{S}\}_{1,1}^{-1}], \tag{19}$$

with the two terms in the square brackets denoting the (1,1) element of the inverse of the matrix $\omega\mathbf{1}-\mathbf{R}$ and $\omega\mathbf{1}-\mathbf{S}$, respectively. Equation (19) is exact and holds for any orientation of the dipoles. Of course, for any reasonable value of N, the actual evaluation has to be numerical, where the most practical way to evaluate the matrix elements of the inverse is not to calculate the inverse but rather, to solve the set $(\omega\mathbf{1}-\mathbf{R})\tilde{\mathbf{X}}(\omega) = \mathbf{X}(t=0)$ and similarly for $\tilde{\mathbf{Y}}$. Results of this analysis will be presented in Sec. IV.

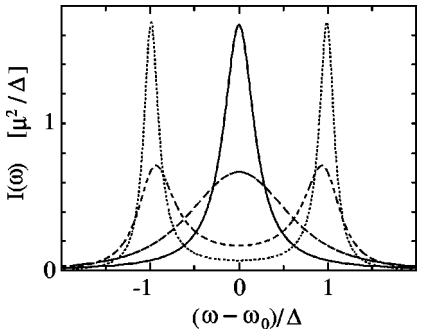

FIG. 2. Absorption spectrum for a monomer with dichotomic noise for $\lambda/\Delta = 5$ (solid line), 2 (long dash), 0.5 (short dash), and 0.2 (dots).

To end this section, it is useful to briefly comment on the situation of a homogeneous aggregate, where $\Delta = 0$. Then, one immediately finds that $\{\omega\mathbf{1}-\mathbf{R}\}_{1,1}^{-1} = 1/[\omega - \Omega_{q=0}]$ and $\{\omega\mathbf{1}-\mathbf{S}\}_{1,1}^{-1} = 1/[\omega - \Omega_{q=1}]$, with

$$\Omega_q = \omega_0 + \sum_{m=\pm 1,\pm 2,\ldots} J(m)\exp(-2\pi i q m/N). \tag{20}$$

This agrees with the well-known fact that the eigenstates for the homogeneous ring are the Bloch functions

$$|q\rangle = \frac{1}{\sqrt{N}}\sum_n \exp(-2\pi i q n/N) b_n^\dagger|0\rangle \tag{21}$$

with wave number q $(=0,1,\ldots,N-1)$ and frequency Ω_q and that only three of these states are dipole allowed. These allowed states are $q = 0$, related to the component of the molecular dipoles perpendicular to the plane of the ring, and $q = 1$ or $N-1$ (degenerate), which are related to the dipole component in the plane of the ring. In this limit, the absorption spectrum thus contains two delta-shaped peaks[26] with relative intensities $\cos^2\beta$ and $\sin^2\beta$.

IV. NUMERICAL RESULTS AND DISCUSSION

Using the equation of motion method described in Sec. III, we numerically evaluated the absorption spectrum for various ring sizes N, dipole orientations, and system parameters Δ/J_0 and λ/J_0. The coefficient matrices $\mathbf{R}$ and $\mathbf{S}$ were automatically generated by FORTRAN routines and the linear equations of motion were solved on IBM RISC/6000 and CRAY machines using standard linear algebra routines.

Before discussing the results for aggregates, it is useful to briefly recall the well-known case of a single molecule with dichotomic noise.[24] Then, the absorption spectrum involves a hierarchy of only two equations, leading to

$$I(\omega) = \frac{\mu^2}{3}\frac{\Delta^2\lambda}{(\omega-\omega_0)^2\lambda^2 + [(\omega-\omega_0)^2 - \Delta^2]^2}. \tag{22}$$

In Fig. 2, this spectrum is plotted for various values of λ/Δ.

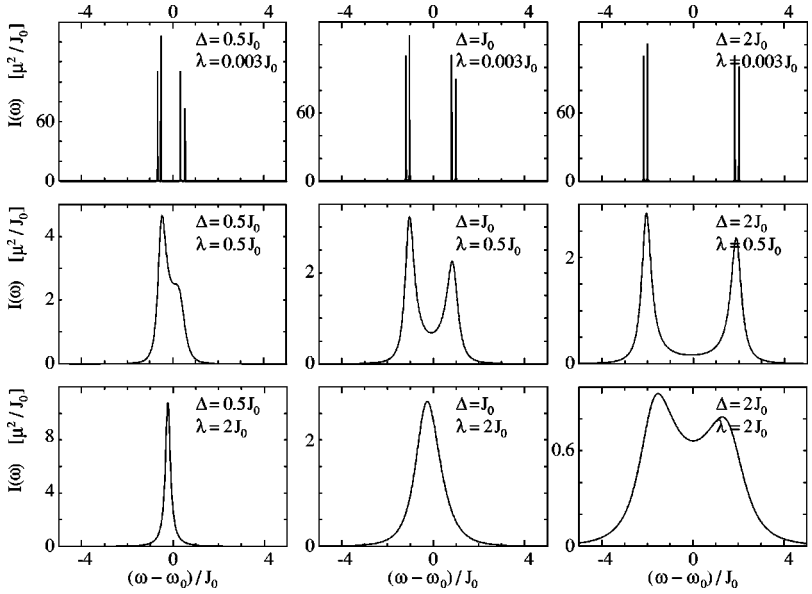

FIG. 3. Exact absorption spectra for the tetramer ($N=4$) with dichotomic noise and dipole orientations $\beta=\pi/2$ and $\alpha=\pi/4$. The parameters Δ/J_0 and λ/J_0 are indicated in the panels.

The features of this figure are well known: for slow fluctuations ($\lambda \ll \Delta$), the spectrum has two narrow Lorentzian lines at $\omega=\omega_0 \pm \Delta$ and a half width at half maximum (HWHM) of $\lambda/2$. For increasing λ/Δ, the peaks broaden and start to merge, while for $\lambda > \sqrt{2}\Delta$, one peak is left, which for increasing fluctuation rate becomes a Lorentzian again with a HWHM Δ^2/λ (motional narrowing).

We now return to aggregates of interacting molecules, in which case J_0 sets a third frequency scale that may be varied. In the examples which we will discuss below, some of the spectral properties are very general (also see spectra for $N \leqslant 6$ in Refs. 19) and may easily be understood physically. First, in the limit of slow fluctuations ($\lambda/\Delta \ll 1$), the spectrum contains a number of narrow peaks, which spread over a larger energy range for increasing Δ/J_0 and which rapidly become more numerous for increasing N. In this limit, each molecule in the ring has a static random frequency offset of $\pm\Delta$ (with equal probability). The various realizations of a ring with such static disorder give rise to different sets of discrete exciton frequencies, which lead to a series of narrow absorption lines. The number of different disorder realizations grows rapidly with increasing ring size, which explains the increasing number of lines for larger rings. Furthermore, for increasing Δ/J_0, the effect of the disorder on the optical selection rules becomes stronger and more of the exciton states are visible in absorption. This explains the spread of the absorption strength over a larger frequency interval. (For $\Delta/J_0 \ll 1$, almost all oscillator strength is concentrated near one of the exciton band edges.)

For increasing λ (keeping Δ and J_0 fixed), the discrete lines broaden and merge (see Fig. 2) to a single rather broad and structured feature at intermediate λ values. For fast fluctuations ($\lambda \gg \Delta$), just as in the monomer case, the whole spectrum collapses to a single motionally narrowed peak. Due to exchange narrowing, spectra in general also narrows for increasing N (keeping all other parameters fixed; see Sec. V).

In Fig. 3, we show spectra for tetramers ($N=4$) with dipole orientations $\beta=\pi/2$ and $\alpha=\pi/4$ for various parameter choices Δ/J_0 and λ/J_0. All dipole–dipole interactions on the ring are included. The current dipole geometry is rather special, as it leads to vanishing nearest-neighbor interactions [see Eq. (2)]. Thus, if we neglect the long-range nature of the dipole–dipole interaction, the spectra for this ring would have the same shape as the monomer spectra in Fig. 2. In Fig. 3, we clearly observe the effects of the long-range interaction, which splits up both narrow monomer lines that occur for slow fluctuations. In fact, the ring now consists of two pairs of noninteracting dimers, from which the spectra are easily understood. In addition to splitting the monomer lines, the long-range interaction (not suprisingly) also leads to a shift compared to the monomer spectra, which is clearly observed for the single peak in the motional narrowing limit ($\Delta=0.5J_0$, $\lambda=2.0J_0$).

In Fig. 4, we show spectra for hexamers ($N=6$) with dipole orientations $\beta=\pi/2$ and $\alpha=0$, i.e., dipoles in the plane of the ring parallel to the ring's tangent. In photosynthetic light harvesting systems, the dipole orientation is close to tangential.[1] Again, we included all dipole–dipole interactions on the ring. First, we note that the general features discussed at the beginning of this section are indeed observed: the number of peaks in the slow fluctuation limit ($\lambda/J_0=0.003$) has indeed increased strongly compared to the tetramer. Yet, for increasing fluctuation rate, all peaks merge to one feature which narrows in the fast-fluctuation limit. These spectra may be compared to the ones obtained in the nearest-neighbor approximation ($k=7/4$ in Ref. 19). One then finds that, again, the long-range interactions shift all spectral features. This is clear in the lower two rows of panels in Fig. 4, which also contain the spectra in the nearest-neighbor approximation. One also observes that the spectral structure is not affected very strongly by including long-range interactions.

In Fig. 5 we show spectra for nonamers ($N=9$) for the same tangential dipole orientation and the same parameter values as in the case $N=6$. All dipole–dipole interactions are included. The effects of the long-range interactions are very similar as in the case $N=6$ and we will not discuss them

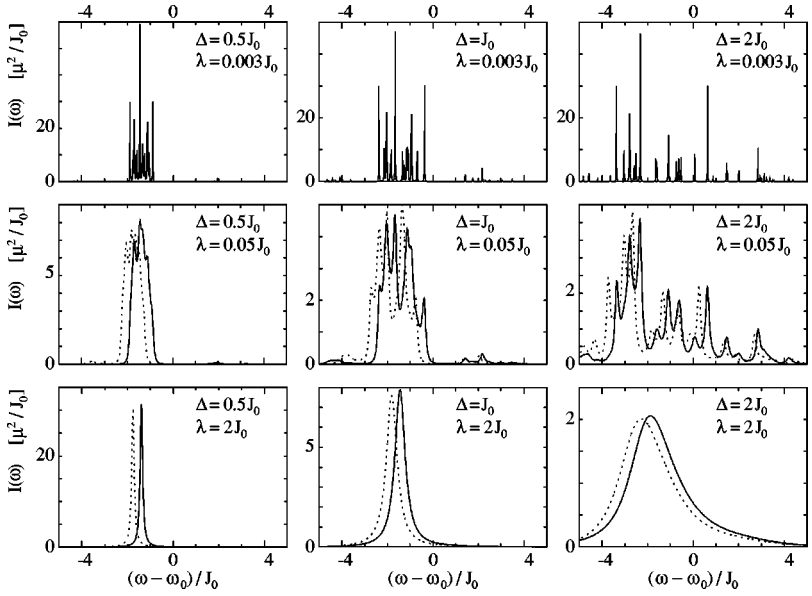

FIG. 4. Exact absorption spectra for the hexamer ($N=6$) with dichotomic noise and dipole orientations $\beta=\pi/2$ and $\alpha=0$ (tangential orientation). The parameters Δ/J_0 and λ/J_0 are indicated in the panels. The dotted lines in the lower two rows of panels give the spectra if we only account for nearest-neighbor interactions.

here. Again, Fig. 5 clearly shows the general spectral properties as a function of Δ/J_0 and λ/J_0. Moreover, we observe that the density of narrow peaks in the case of slow fluctuations has now increased so much (due to the system size) that they begin to merge to a single feature. At small disorder, this peak is concentrated in an interval of the order 2Δ near the frequency of the optically allowed exciton state $|q=1\rangle$ that exists for $\Delta=0$ (for the present dipole orientations, that is at $\approx -2.8J_0$). For increasing disorder, the absorption spectrum spreads over the entire exciton band. Comparison to Fig. 4 shows that the larger system size also leads to shifts of the spectral features. This is a consequence of: (i) the inclusion of long-range interactions (a larger system implies more interactions) and (ii) the fact that for the current dipole orientation, the interactions still rather strongly depend on N through the orientation factor in Eq. (2). It should be noted, however, that for growing λ/J_0, the *shape* (and in particular the width) of the spectrum becomes less sensitive to N. Size saturation is a well-known phenomenon for linear and nonlinear aggregate spectra and results from any type of line broadening mechanism (whether homogeneous or inhomogeneous).[27–30] In our case of dynamic disorder, one may say that the fluctuation rate imposes a natural size scale ($\sim\sqrt{8J_0/\lambda}$ for nearest-neighbor interactions if $\lambda/J_0 \ll 4$)[20] over which the excitons in the fluctuating aggregate may still be considered as effective, fully delocalized adiabatic exciton states. For larger system sizes, the effective exciton does not see the entire ring anymore and the spectrum saturates. In Sec. V we will discuss this saturation in more detail for the widths of the absorption peaks.

Finally, in Fig. 6, we show results for dodecamers ($N=12$) again for the tangential dipole orientation and the same parameter values as for $N=6$ and $N=9$. The trends mentioned in the discussion above are further confirmed, in particular, the spectra for $\lambda > J_0$ have now saturated completely:

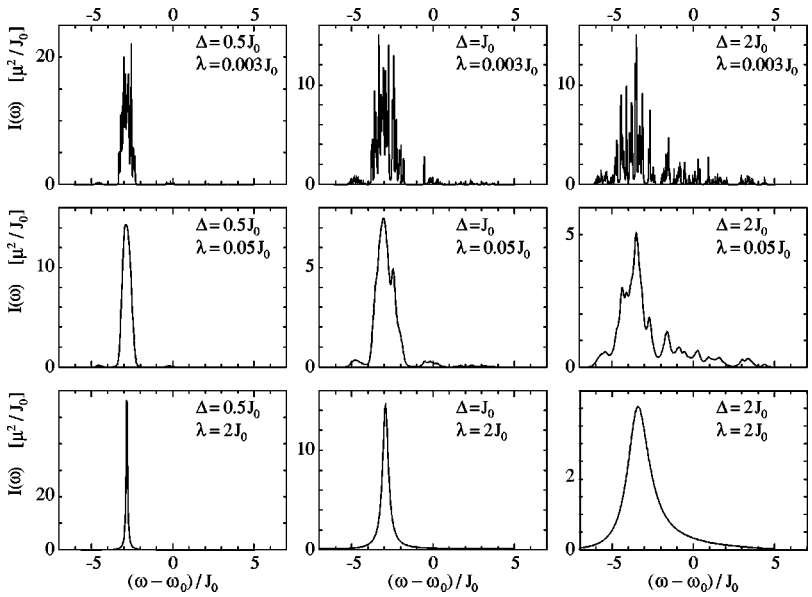

FIG. 5. As Fig. 4, but now for the nonamer ($N=9$).

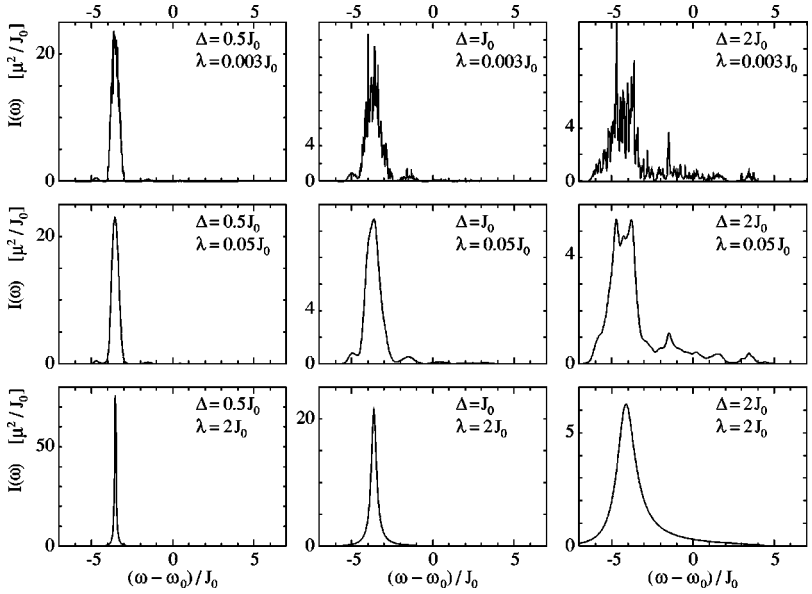

FIG. 6. As Fig. 4, but now for the dodecamer ($N=12$).

they only shift relative to $N=9$, but they do not (for all practical purposes) change shape anymore. A similar saturation also sets in at smaller λ values already, as is clear from the panels for $\lambda/J_0=0.05$, $\Delta/J_0=0.5$ or 1.0 in Figs. 5 and 6. This saturation reduces the necessity to investigate much larger system sizes. On the other hand, it should be noted that $N=12$ is about the maximum size that we presently can, reasonably speaking, handle exactly. For larger sizes, the memory it takes to store the matrix **R** or **S** becomes a problem. This might be solved by using iterative sparse-matrix routines (both matrices are sparse as is easily seen) but such routines are not standard for nonhermitian complex matrices like **R** and **S**.

V. EXCHANGE NARROWING AND RPA

In this section, we analyze the width and (in less detail) the position of the single absorption feature that arises if the fluctuations become faster. Generally speaking, two distinct narrowing effects play an important role in determining the linewidths. The first is known as motional narrowing. This is a well-known single-molecule effect: for fast fluctuations ($\lambda \gg \Delta$) the absorption experiment averages very efficiently over the various possible phase evolutions $\{\int dt[\omega_0 + \Delta(t)]\}$ of the molecular transition dipole dictated by the different realizations of the stochastic process $\Delta(t)$. The faster the fluctuations are, the smaller the spread in realized phases at any particular time will be. This also implies that the absorption spectrum becomes narrower (see Fig. 2); the linewidth decreases according to Δ^2/λ.[24] This behavior is not limited to dichotomic disorder: it occurs in the fast-fluctuation regime of any Markov process with second moment given by Eq. (4), and in particular also for the Gauss–Markov process.

The second narrowing phenomenon is exchange narrowing, which results from the excitation transfer (or exchange) interactions $J(m)$. As a result of these interactions, the excitations delocalize over a number of molecules. If the disorder on these molecules is uncorrelated (as we assumed), this obviously leads to a more efficient averaging over the possible evolutions of the excitation's phase, which in turn leads to a narrower absorption spectrum. Exchange narrowing is well known for the case of static disorder,[31,32] but recently, we showed that it may also occur on top of the motional narrowing effect in the case of fast fluctuations.[20] For small aggregates, the latter exchange narrowing was found to take place with a factor of N, until a saturation ring size ($\sim\sqrt{8J_0/\lambda}$ if $\lambda/J_0 \ll 4$) is reached above which the spectrum does not change anymore. As Ref. 20 was limited to dipoles oriented perpendicular to the plane of the aggregate and accounted for nearest-neighbor interactions only, in this section we investigate how the more general conditions of the present paper affect the exchange narrowing of fast fluctuations.

From the various figures in Sec. IV, one finds that for dipoles oriented in the plane of the aggregate, the spectrum also tends to narrow with increasing ring size (other parameters fixed). To illustrate this more clearly, Fig. 7 contains absorption line shapes for $\Delta=\lambda=0.5J_0$ for aggregates of various sizes, with dipoles oriented tangentially to the ring:

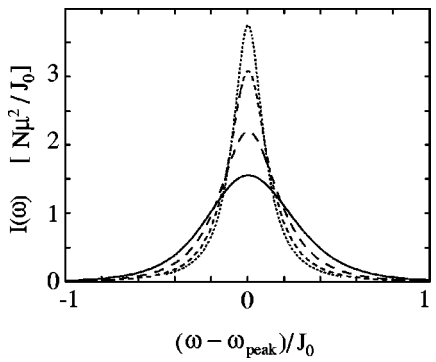

FIG. 7. Absorption peaks for ring aggregates with tangential dipole orientation ($\beta=\pi/2$ and $\alpha=0$) for $N=4$ (solid line), 6 (long dash), 9 (short dash), and 12 (dots). The peaks have been shifted so that their maxima occur at the same position. In all cases, $\Delta=\lambda=0.5J_0$. Long-range dipole–dipole interactions are included.

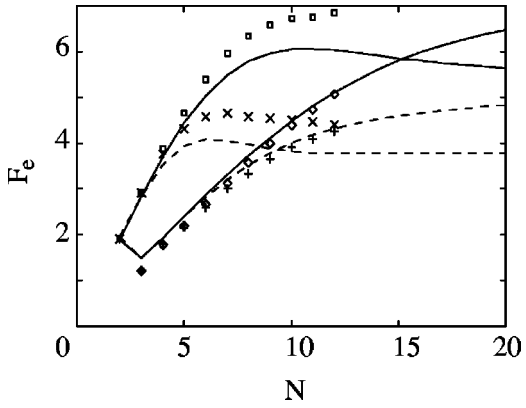

FIG. 8. Exchange narrowing factor F_e as a function of aggregate size N for $\Delta=\lambda=0.5J_0$. Symbols denote the exact (numerical) results for dipoles perpendicular to the ring with nearest-neighbor interactions ($\times$), idem with long-range interactions ($\square$), dipoles tangential to the ring with nearest-neighbor interactions ($+$), and idem with long-range interactions ($\diamond$). Curves give the corresponding semianalytical results obtained from the random-phase approximation discussed in Sec. V.

$\alpha=0,\beta=\pi/2$. We note that to facilitate comparison, the spectra have been shifted such that they have a common maximum. The actual peak position (exciton band edge) still has an appreciable N dependence, as we already explained in Sec. IV (see discussion of the $N=9$ case). From Fig. 7 one clearly observes that with increasing ring size, the absorption line indeed narrows. Quantitatively, however, important differences occur compared to the exchange narrowing for dipoles oriented in the z direction.[20] This is clearly seen in Fig. 8, where we show the exchange narrowing factor, defined as

$$F_e=\frac{\Delta^2}{\lambda W}, \tag{23}$$

with W the HWHM of the absorption peak. Shown (as symbols) are the values for F_e obtained from the exact spectra for ring sizes up to $N=12$ in four different cases: dipoles oriented perpendicular to the plane of the ring, with long-range interactions and with nearest-neighbor interactions only, and similarly for dipoles oriented tangentially to the ring. The numerical errors in F_e are $\leqslant 2\%$. The curves in Fig. 8 represent the random phase approximation (see below) for these various cases.

We start our discussion for dipoles oriented perpendicular to the ring and keeping only nearest-neighbor interactions $J(m=\pm 1)$ (indicated by $\times$ in Fig. 8). The plot clearly shows that for small aggregates, F_e equals the ring size, while for larger sizes a saturation occurs. In Ref. 20, this small-aggregate limit was explained using perturbative arguments: to first order in the disorder, the completely delocalized optically active $q=0$ exciton undergoes a frequency fluctuation $\Delta_{q=0}(t)$ that is the average of the N molecular fluctuations. The second moment of this stochastic process is identical to that of a single molecule [see Eq. (4) with $m=n$] except that the amplitude Δ is replaced by $\Delta/\sqrt{N}$. In the fast-fluctuation regime, where the linewidth is proportional to the amplitude squared, this immediately leads to $F_e=N$. For increasing N, however, one reaches a point where the exciton cannot be considered to adiabatically follow all fluctuations in the ring anymore and the exchange narrowing saturates. For nearest-neighbor interactions this saturation was shown to occur at[20]

$$N=F_e^{\infty}=\sqrt{\frac{2\lambda^2+32\ J_0^2}{\lambda^2+\lambda\sqrt{\lambda^2+16J_0^2}}}, \tag{24}$$

which for the current parameters ($\lambda=0.5J_0$) equals ~ 4. This is in good agreement with Fig. 8.

Next, we consider the case of dipoles perpendicular to the ring, but now with long-range interactions ($\square$ in Fig. 8). For small N, the behavior is identical to the case of nearest-neighbor interactions: the fully delocalized $q=0$ exciton is still the relevant eigenstate. The saturation is seen to occur at larger ring size, however, and with a larger narrowing factor (actually, the exact results just seem to saturate at $N=12$). This also is to be expected: the long-range interactions facilitate the complete delocalization of the exciton and postpone the size saturation.

We now turn to the case of dipoles oriented tangentially to the ring ($+$ in Fig. 8). For small N, we now observe that $F_e\approx N/2$. The extra factor of 1/2 can be traced back to the fact that for this dipole orientation, in the limit $\Delta=0$, two degenerate dipole allowed excitons exist ($q=1$ and $q=N-1$). This degeneracy is lifted by finite fluctuations, so that the unperturbed absorption line is split, leading to an effective broadening. Using degenerate perturbation theory, one finds that the two-time correlation functions of the eigenvalues after the splitting both have an amplitude $2\Delta^2/N$, which agrees with the observed factor of 1/2. It should be noted that for $N=2$, no degeneracy occurs ($N-1=1$ then), which explains why in Fig. 8 the factor of 1/2 is not observed for this ring size (all exact data points fall on top of each other for $N=2$). It is also seen from Fig. 8 that for the tangential dipole orientation saturation has set in, but has not really been fully reached at $N=12$. The explanation why saturation takes longer than in the case of dipoles oriented perpendicular to the ring is that (for N not too small) the orientation factor in Eq. (2) increases the magnitude of the nearest-neighbor interaction by a factor of 2 for the tangential orientation, so that it is easier to maintain full exciton delocalization against the disorder fluctuations.

Finally, the effects of including the long-range interactions for the tangential orientation are similar to those for the perpendicular orientation: the small-aggregate behavior is unchanged, while the saturation occurs at a larger aggregate size. These effects are clearly observed in Fig. 8 ($\diamond$).

All spectra and spectral widths studied thus far are exact. As, however, the exact analysis involves a numerical effort that rapidly increases with N, it is useful to have approximate semianalytical expressions for the spectrum, its width, and its position. In the remainder of this section we will derive such expressions within the random-phase approximation (RPA). Not only do the results give insight into the spectra for ring sizes that are too large to allow for exact solutions, they also help one to understand in a simple way the exact results obtained for smaller rings.

In the RPA, one truncates the hierarchy of 2^N equations of motion by the factorization $\langle U_{0n}(t)\Delta_{n_1}(t)\Delta_{n_2}(t)\rangle$

$=\langle U_{0n}(t)\rangle\langle \Delta_{n_1}(t)\Delta_{n_2}(t)\rangle$, which is believed to be a good approximation for $\Delta<\sqrt{2}\lambda$, i.e., in the fast-fluctuation regime.[12,19] We note that this factorization approximation gives identical results for any Markov process with two-time correlation function given by Eq. (4). Thus, in particular, all results derived in the remainder of this section also hold for Gauss–Markov noise.

After the truncation, the matrix $\mathbf{R}$ reduces to a matrix $\mathbf{R}'$ of dimension $N+1$ in the subspace of $X^{(0)}$ and $X^{(1)}(n)(n=0,\ldots,N-1)$:

$$\mathbf{R}'=\begin{pmatrix}\Omega_{q=0} & \mathbf{A}\\ \mathbf{A}^T & \mathbf{B}\end{pmatrix}. \tag{25}$$

Here, Ω_q is as defined in Eq. (20), $\mathbf{A}$ is the N-dimensional vector $(\Delta,0,\ldots,0)$, while $\mathbf{B}$ is the $N\times N$ matrix that has $\omega_0-i\lambda$ as its diagonal elements, and $B_{nm}=J(n-m)$ for $n\neq m$. The matrix $\mathbf{B}$ is equivalent to the Hamiltonian for a homogeneous ring of N molecules with long-range interactions and effective transition frequency $\omega_0-i\lambda$.

Similarly, the matrix $\mathbf{S}$ reduces to a matrix $\mathbf{S}'$ of dimension $N+1$:

$$\mathbf{S}'=\begin{pmatrix}\Omega_{q=1} & \mathbf{A}\\ \mathbf{A}^T & \mathbf{C}\end{pmatrix}. \tag{26}$$

Here, $\mathbf{C}$ is the $N\times N$ matrix that has $\omega_0-i\lambda$ as its diagonal elements, and $C_{nm}=J(n-m)\exp[-2\pi i(n-m)/N]$ for $n\neq m$.

Due to their translational symmetry, the matrices $\mathbf{B}$ and $\mathbf{C}$ are easily diagonalized which, using Eq. (19) in a straightforward way, leads to the RPA spectrum:

$$I(\omega)=-\frac{N}{3}\mathrm{Im}\left(\frac{\mu_z^2}{\omega-\Omega_{q=0}-\Sigma(\omega)}+\frac{\mu_{xy}^2}{\omega-\Omega_{q=1}-\Sigma(\omega)}\right), \tag{27}$$

with

$$\Sigma(\omega)=\frac{\Delta^2}{N\lambda}\sum_{q=0}^{N-1}\frac{\lambda}{\omega-\Omega_q+i\lambda}, \tag{28}$$

the complex and frequency dependent exciton self-energy. Note that both the z and the xy part of the spectra are governed by the same self-energy.

If we restrict ourselves to nearest-neighbor interactions J, the sum in the self-energy can be evaluated analytically[33,34] giving:

$$\Sigma_{\mathrm{near}}(\omega)=\frac{\Delta^2}{2J}\frac{2}{a-a^{-1}}\frac{1+a^{-N}}{1-a^{-N}}, \tag{29}$$

with $a=\delta\pm\sqrt{\delta^2-1}$ (sign chosen such that $|a|>1$) and $\delta=(\omega-\omega_0+i\lambda)/2J$. Note that for $N\to\infty$, the last factor tends to unity, a limit that may also be obtained by converting the sum over q in Eq. (28) to an integral.

We now return to the general case of long-range interactions. A further simplification of the spectrum [Eq. (27)] is obtained by applying the pole approximation, in which one replaces $\Sigma(\omega)$ by $\Sigma(\Omega_{q=0})$ in the first term and by $\Sigma(\Omega_{q=1})$ in the second term. The spectrum then consists of two Lorentzians centered at $\Omega_{q=0}+\mathrm{Re}\,\Sigma(\Omega_{q=0})$ and $\Omega_{q=1}+\mathrm{Re}\,\Sigma(\Omega_{q=1})$, respectively, and with widths (HWHM) of $-\mathrm{Im}\,\Sigma(\Omega_{q=0})$ and $-\mathrm{Im}\,\Sigma(\Omega_{q=1})$, respectively. For large N, these peaks tend towards each other. Generally, pole approximations are good for narrow absorption peaks in which the replacement of $\Sigma(\omega)$ by a constant is reasonable. Thus, one expects the approximation to improve for faster fluctuations and (or) larger aggregates.

TABLE I. Comparison of the absorption peak position $[(\omega_{\mathrm{peak}}-\omega_0)/J_0]$ for $\Delta=\lambda=0.5J_0$ according to exact numerical calculation and RPA for two different dipole orientations: tangential ($\beta=\pi/2,\alpha=0$) and perpendicular ($\beta=0$). All dipole–dipole interactions on the ring are included. Absolute numerical errors in the exact data are 0.003.

	Tangential		Perpendicular	
N	Exact	RPA	Exact	RPA
4	0.328	0.3441	2.428	2.4136
6	−1.412	−1.4104	2.593	2.5849
9	−2.841	−2.8358	2.604	2.6011
12	−3.540	−3.5361	2.588	2.5878

From the widths calculated in the pole approximation, we find the following exchange narrowing factors:

$$F_{\mathrm{e}}^{z}=N\left(\sum_{q=0}^{N-1}\frac{\lambda^2}{(\Omega_q-\Omega_0)^2+\lambda^2}\right)^{-1} \tag{30}$$

and

$$F_{\mathrm{e}}^{xy}=N\left(\sum_{q=0}^{N-1}\frac{\lambda^2}{(\Omega_q-\Omega_1)^2+\lambda^2}\right)^{-1}. \tag{31}$$

These results are plotted as curves in Fig. 8 for the four cases which we also studied by exact solution. Taking into account the fact that for $\Delta=\lambda=0.5J_0$ one is just on the edge of the fast-fluctuation regime, the agreement with the exact results is good. In particular, for $N\ll 2\pi\sqrt{J_0/\lambda}$, one easily shows from Eqs. (30) and (31) that, indeed, $F_{\mathrm{e}}^{z}\approx N$ (only the term with $q=0$ contributes considerably), while $F_{\mathrm{e}}^{xy}\approx N/2$ (both the terms with $q=1$ and $q=N-1$ contribute). The degeneracy effect in F_{e}^{xy}, which we already argued above, is thus seen explicitly in the RPA.

Above, we concentrated on an analysis of the linewidths, which are of most interest because of the narrowing phenomena. We will not discuss the line positions in any detail here. Suffice it to mention that the line shifts in the exact spectra caused by changing dipole orientations, ring size, or number of neighbors accounted for, are for $\Delta\leqslant\lambda$ well described by the RPA within the pole approximation. As an illustration, Table I gives the exact and RPA peak positions at $\Delta=\lambda=0.5J_0$ for various aggregate sizes for both the tangential and the perpendicular dipole orientations in case all dipole–dipole interactions are accounted for.

VI. CONCLUDING REMARKS

In this paper, we studied the optical absorption spectrum of molecular ring aggregates with dichotomic dynamic disorder. We followed the main idea of Refs.18 and 19 that for dichotomic noise one may derive the absorption spectrum through closed hierarchies of equations of motion. We

showed that for ring aggregates dynamic variables can be defined such that the hierarchies contain 2^N equations of motion. This is a factor of N less than what has been used before. We also showed that two such hierarchies suffice to calculate the spectrum for arbitrary orientations of the molecular transition dipoles in the ring and that these two hierarchies are, in fact, very similar. We explicitly accounted for the possibility of long-range (dipole–dipole) transfer interactions.

Using this technique, we evaluated exact absorption spectra for rings of up to $N=12$ molecules. We found that including long-range interactions has a strong effect on peak positions. Moreover, it generally postpones saturation of the spectrum to the long-chain limit. We particularly focused on the effect of exchange narrowing of fast fluctuations, where the spectrum consists of one or two sharp peaks. The exact calculations show that the dipole orientation and the inclusion of long-range interactions quite strongly influence the exchange narrowing factor. These effects are physically well understood. We also considered the RPA, which yields a closed expression for the spectrum in the fast-fluctuation regime.

We showed explicit results for two extreme types of dipole orientation: either perpendicular to the plane of the ring or in the plane of the ring. Then, only one of the two different hierarchies contributes to the spectrum. Intermediate cases are not more complicated to evaluate: they involve solving both hierarchies with the appropriate dipolar interactions and adding their contributions.

In spite of the complexity of its analysis, the model we used to account for the aggregate's environment (one-component dichotomic noise) cannot be expected to give a detailed description of such complicated systems as light-harvesting complexes or *J* aggregates in solution. Ideally, one should deal with some of the environment degrees of freedom (vibrations) explicitly.[35] However, for strongly coupled molecules in aggregates larger than dimers, this approach is almost prohibitively complicated.[36] Alternatively, a big step forward in the modeling would be the inclusion of a static Gaussian disorder component in addition to our dynamic dichotomic one. Recent absorption and photon echo experiments on *J* aggregates of TDBC (5,5′,6,6′-tetrachloro-1,1′-diethyl-3,3′-bis(4-sulfobutyl)-benzimiclazolo carbocyanine) in solution have given clear evidence for such a combination of slow (static) and fast fluctuation processes.[37] Unfortunately, performing exact calculations for such a two-component disorder is much more involved than for the model we analyzed. A straightforward approach is to simulate the static disorder and then for each disorder realization build a hierarchy to account for the dynamic component. For two reasons, however, this is a very time-consuming calculation: (i) the static disorder breaks the translational symmetry in the hierarchy and forces one to consider a set of $N2^N$, instead of 2^N, equations of motion; (ii) to sample the disorder, many different realizations of this hierarchy must be solved.

Yet, one interesting observation about this two-component disorder can readily be made. Let us suppose that for a particular disorder realization the exciton states of the Hamiltonian without the dynamic disorder component read: $|k\rangle=\Sigma_n a_{kn} b_n^\dagger|0\rangle$, with k some quantum label and a_{kn} the real exciton amplitude on molecule n. If one now treats the dynamic disorder component in a perturbative way, the two-time correlation function of the stochastic frequency fluctuation of state $|k\rangle$ reads

$$\langle \Delta_k(t)\Delta_k(\tau)\rangle = \Delta^2 \sum_n a_{kn}^4 \exp(-\lambda|t-\tau|). \tag{32}$$

As a consequence, for fast fluctuations the linewidth related to the dynamic component has an exchange narrowing factor $\Sigma_n a_{kn}^4$. Performing the average over the realizations of the static disorder then yields $F_e=N_{\mathrm{del}}$, where N_{del} is the participation ratio $\langle \Sigma_n a_{kn}^4\rangle_{\mathrm{static}}$, which is a well-known measure of the exciton delocalization length due to static disorder.[38,39] Thus, adding static disorder changes the scaling of the exchange narrowing factor with the aggregate size N to a scaling with N_{del}. This intuitively appealing result also implies that the homogeneous dephasing time of the aggregate, as measured in hole burning or photon echoes, scales proportional to N_{del}. Of course, this only holds as long as the saturation size dictated by the dynamic component is larger than N_{del}, as otherwise the perturbative treatment is not justified. In particular, in the white-noise limit ($\lambda \gg \Delta, J_0$), the saturation size is just one molecule [see Eq. (24)] and the homogeneous dephasing rate is, independent of the static disorder, given by the well-known single molecule result λ/Δ^2.[24,14]

We finally note that for *linear* aggregates (open boundary conditions) with one-component dichotomic disorder, the closed hierarchy cannot be reduced to 2^N equations, as the translational symmetry is broken.[19] Straightforward perturbative treatment of the disorder indicates that now exchange narrowing in the fast-fluctuation regime takes place with a factor $2(N+1)/3$ (nearest-neighbor interactions only; see Ref. 32). This is confirmed within the RPA, which also shows that, as physically expected, the saturation size does not depend on the boundary conditions and is still given by Eq. (24).[40]

ACKNOWLEDGMENTS

The authors thank Martijn Wubs for many useful discussions, Dr. Steven Pickering for help in the numerical calculations, and Dr. Gediminas Juzeliūnas for pointing out Refs. 33 and 34.

[1] X. Hu and K. Schulten, Phys. Today **50**(8), 28 (1997), and references therein.
[2] T. Pullerits, M. Chachisvilis, and V. Sundström, J. Phys. Chem. **100**, 10787 (1996).
[3] J. A. Leegwater, J. Phys. Chem. **100**, 14 403 (1996).
[4] K. Sauer, R. J. Cogdell, S. M. Prince, A. A. Freer, N. W. Isaacs, and H. Scheer, Photochem. Photobiol. **64**, 564 (1996).
[5] T. Meier, V. Chernyak, and S. Mukamel, J. Phys. Chem. **101**, 7332 (1997).
[6] P. W. Anderson and P. R. Weiss, Rev. Mod. Phys. **25**, 269 (1953).
[7] R. Kubo, J. Phys. Soc. Jpn. **9**, 935 (1954).
[8] H. Haken and G. Strobl, Z. Phys. **262**, 135 (1973).
[9] H. Sumi, J. Chem. Phys. **67**, 2943 (1977).
[10] A. Blumen and R. Silbey, J. Chem. Phys. **69**, 3589 (1978).
[11] I. B. Rips and V. Cápek, Phys. Status Solidi B **100**, 451 (1980).
[12] A. M. Jayannavar, B. Kaiser, and P. Reineker, Z. Phys. B **77**, 229 (1989).
[13] H. Ezaki and F. Shibata, Physica A **192**, 124 (1993); **192**, 137 (1993).

[14] S. Mukamel, *Principles of Nonlinear Optical Spectroscopy* (Oxford University Press, Oxford, 1995).
[15] V. Chernyak and S. Mukamel, J. Chem. Phys. **105**, 4565 (1996).
[16] E. T. J. Nibbering, D. A. Wiersma, and K. Duppen, Phys. Rev. Lett. **66**, 2464 (1991); Chem. Phys. **183**, 167 (1994).
[17] P. Reineker, in *Exciton Dynamics in Molecular Crystals and Aggregates*, edited by G. Höhler (Springer, Berlin, 1988).
[18] B. Kaiser, A. M. Jayannavar, and P. Reineker, J. Lumin. **43**, 73 (1989); P. Reineker, B. Kaiser, A. M. Jayannavar, and V. Kapsa, *ibid.* **45**, 238 (1990).
[19] P. Reineker, Ch. Warns, Th. Neidlinger, and I. Barvík, Chem. Phys. **177**, 715 (1993); Ch. Warns, I. Barvík, P. Reineker, and Th. Neidlinger, *ibid.* **194**, 117 (1995); I. Barvík, P. Reineker, Ch. Warns, and Th. Neidlinger, J. Lumin. **65**, 169 (1995).
[20] M. Wubs and J. Knoester, Chem. Phys. Lett. **284**, 63 (1998).
[21] A. S. Davydov, *Theory of Molecular Excitons* (Plenum, New York, 1971).
[22] V. M. Agranovich and M. D. Galanin, *Electronic Excitation Energy Transfer in Condensed Matter*, edited by V. M. Agranovich and A. A. Maradudin (North Holland, Amsterdam, 1982).
[23] R. C. Bourret, U. Frisch, and A. Pouquet, Physica (Amsterdam) **65**, 303 (1973).
[24] R. Kubo, Adv. Chem. Phys. **15**, 101 (1969).
[25] V. E. Shapiro and V. M. Loginov, Physica A **91**, 563 (1978).
[26] In this limit the imaginary part is generated by adding $+i0^+$ in the frequency denominators, as is usual for Green functions.
[27] F. C. Spano and S. Mukamel, Phys. Rev. Lett. **66**, 1197 (1991); J. Chem. Phys. **95**, 7526 (1991).
[28] H. Ishihara and K. Cho, Phys. Rev. B **42**, 1724 (1990).
[29] F. C. Spano, Chem. Phys. Lett. **220**, 365 (1994).
[30] H. Fidder, J. Knoester, and D. A. Wiersma, J. Chem. Phys. **95**, 7880 (1991).
[31] E. W. Knapp, Chem. Phys. **85**, 73 (1984).
[32] J. Knoester, J. Chem. Phys. **99**, 8466 (1993).
[33] E. Montroll, J. Math. Phys. **10**, 753 (1969).
[34] K. Lakatos-Lindenberg, R. P. Hemenger, and R. M. Pearlstein, J. Chem. Phys. **56**, 4852 (1972).
[35] T. Renger and V. May, Phys. Rev. Lett. **78**, 3406 (1997).
[36] O. Kühn, T. Renger, V. May, J. Voigt, T. Pullerits, and V. Sundström, Trends Photochem. Photobiol. **4**, 213 (1997).
[37] M. van Burgel, D. A. Wiersma, and K. Duppen, J. Chem. Phys. **102**, 20 (1995).
[38] D. J. Thouless, Phys. Rep. **13**, 93 (1974).
[39] M. Schreiber and Y. Toyozawa, J. Phys. Soc. Jpn. **51**, 1537 (1982).
[40] M. Wubs and J. Knoester (unpublished).